



## Quantification of sliding-induced phase transformation in N3FC diamond-like carbon films

A. M'ndange-Pfupfu<sup>a,\*</sup>, O. Eryilmaz<sup>b</sup>, A. Erdemir<sup>b</sup>, L.D. Marks<sup>a</sup>

<sup>a</sup> Northwestern University, Department of Materials Science and Engineering, 2220 N. Campus Drive, Cook Hall Room 2036, Evanston, IL 60208, United States

<sup>b</sup> Argonne National Laboratory, Energy Systems Division, Tribology Section, 9700 S. Cass Avenue, Argonne, IL 60439, United States

### ARTICLE INFO

#### Article history:

Received 17 September 2010

Received in revised form 19 June 2011

Accepted 25 June 2011

Available online 13 July 2011

#### Keywords:

Diamond-like carbon

Tribochemistry

*In situ* TEM

Tribology

### ABSTRACT

We investigate magnetron-sputtered “N3FC” diamond-like carbon films at the nanoscale using an *in situ* transmission electron microscopy sliding experiment. We measure the sliding-induced changes in  $sp^3$ - and  $sp^2$ -hybridized carbon using electron energy loss spectroscopy, taking into account the effect of the electron beam. The rate of the phase transformation from  $sp^3$  to  $sp^2$  bonding is quantified as being between 0.009% and 0.018% volume transformed per sliding pass.

© 2011 Elsevier B.V. All rights reserved.

### 1. Introduction

The field of tribology has seen significant advances in recent years. With new theoretical models and experimental techniques, the friction and wear behavior of materials has become easier to predict and manipulate, to the benefit of many applications. However, many obstacles still remain. One well-known problem with many tribology experiments is the inability to dynamically observe and measure the processes occurring at the sliding interface. *Post facto* analysis is useful, but rarely does it tell the whole story. A better understanding and characterization of the fundamental mechanical and chemical processes at work can only increase our ability to design and operate better devices.

Another obstacle facing tribologists today is the issue of scale. As the desirable device size shrinks, the surface-to-volume ratio increases, and not only do friction and wear effects become more noticeable, the material behavior can be significantly altered. Surface lubrication is one example: typical liquid lubricants become more and more unfeasible with smaller device dimension, leading to an increased interest in solid coatings for low-friction performance. In this study we will investigate the sliding behavior of diamond-like carbon (DLC) thin films, which can show desirable tribological characteristics depending on the deposition method and testing environment.

DLC is an amorphous form of carbon that consists of a variable composition of  $sp^3$  bonded (tetrahedral) carbon,  $sp^2$  bonded (trigonal) carbon, and hydrogen, ranging up to “pure” tetrahedral amorphous

carbon (ta-c) with 100%  $sp^3$  bonding [1]. The significant fraction of diamond-like bonding – as well as the presence of hydrogen as a passivating agent – results in a hard and chemically nonreactive surface, which contributes to a high resistance to adhesive and abrasive wear. In addition, the ability to form a transfer film during sliding can reduce wear and increase lifetimes in sliding experiments [2,3]. The combination of good mechanical and tribological properties makes DLC an attractive coating option for a variety of applications.

Extensive research has been carried out on the tribological behavior of DLC coatings [4–6]. The results of these studies highlight an important point – that the chemistry (both environment and internal) plays a significant role in the coating performance. By varying the environment and the hydrogen content of the film, the coefficient of friction and wear rate can change by several orders of magnitude [2,7–14]. Molecular dynamics simulations show that the tribochemistry of these films has a large effect on the frictional forces at small scales [15,16]. Increases in the  $sp^2/sp^3$  bonding ratio after tribotesting have been observed in several macroscale experiments [17–21] and called graphitization due to the observation of graphitic wear particles *post facto*. This suggests that performance depends not only on initial composition, but also on sliding-induced changes. Therefore, we need to take a closer, more fundamental look at the structural and chemical changes of DLC films during sliding in order to predict the long-term behavior.

There are several proposed mechanisms for the low friction of hydrogenated DLC films. One possibility is hydrogen termination minimizing adhesive contact, another is the formation of graphitic material either at the surface or within the transfer layer. Less clear is to what extent the  $sp^2$  bonding is amorphous, disordered, or true ordered graphite. In this note we use *in situ* transmission electron

\* Corresponding author. Tel.: +1 847 4917809; fax: +1 847 4917820.

E-mail address: [ariel@u.northwestern.edu](mailto:ariel@u.northwestern.edu) (A. M'ndange-Pfupfu).

microscopy (TEM) to carefully investigate the dynamic changes in carbon bonding during a sliding experiment. We demonstrate that for the conditions of our experiment only disordered  $sp^2$  forms, not crystalline graphite, and that the  $sp^2$  content is proportional to the number of sliding passes.

## 2. Experimental method

### 2.1. Sample preparation

We used a Nanofactory Scanning Tunneling Microscopy (STM) TEM sample holder, as shown in detail in Fig. 1, to perform the experiment *in situ* inside a Tecnai F20ST TEM at 200 kV and approximately  $10^{-7}$  Torr; many details are similar to earlier work with the same system [21–25]. Post-specimen electrons were collected using a Gatan Imaging Filter (GIF). This allowed us to visually observe the sliding in real time, simultaneously record diffraction patterns for structural analysis, and use the GIF to separate electrons by energy, enabling real-time chemical analysis by electron energy-loss spectroscopy (EELS) [26,27].

As shown in Fig. 2, the samples were mounted on standard-sized TEM grids at a  $45^\circ$  angle to horizontal, and the STM probe tip approached horizontally, controlled by stick-slip motion of the sapphire ball as well as a piezoelectric tube. The probe tips, e.g. Fig. 3, were electrochemically etched to a sharp point from 0.25 mm tungsten wire using a solution of 0.5–5 N NaOH. N3FC “nearly frictionless carbon” thin films were prepared at Argonne National Laboratory using a magnetron sputtering process. The films were deposited onto an NaCl crystal random cutting [28], which was then dissolved in water and the film transferred to a copper TEM grid with a lacey carbon film support. The film thicknesses were measured by EELS to be 30–35 nm by the standard log/log relative method [29]. Typical micrographs and EELS spectra of film pre-sliding can be seen in Figs. 4 and 5.

### 2.2. In situ sliding procedure

The sliding experiment was performed by manually approaching the sample until contact was made, and then rastering the tip back and forth using the piezo tube. Given the approximate 800–900 nm range of the motion, and a cycle speed of one per second, the sliding speed was estimated to be  $2 \mu\text{m/s}$ . Before and after the experiment, nanodiffraction patterns were recorded to look for significant structural changes during the experiment. These diffraction patterns

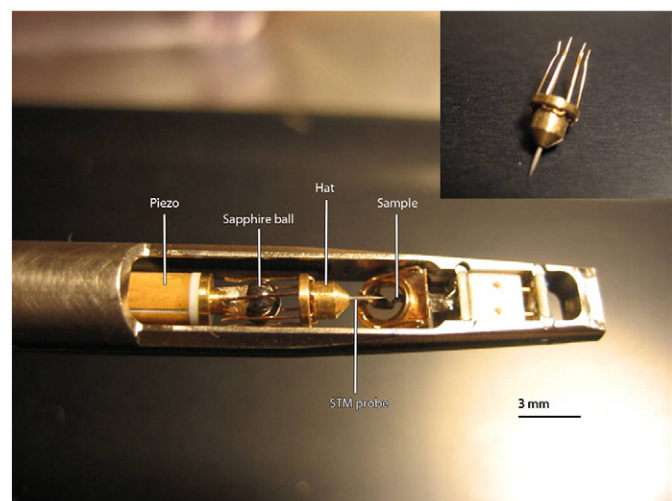


Fig. 1. A closeup of the Nanofactory STM-TEM holder. The piezoelectric tube is used for fine movement control, and the sapphire ball provides coarse stick-slip control.

sampled a circular area approximately 800 nm in diameter around the sliding region. For completeness, we note that due to well-known projection issues with amorphous or highly disordered materials it is unwise to overinterpret minor changes in image or diffraction pattern details, only major ones (e.g. the formation of crystals  $>2$  nm) are detectable.

For all sliding experiments, the maximum contact pressure was estimated using a Hertzian contact model. Because no actual forces are measured in the experiment, we consider this an upper bound estimation based on the literature values for Young's modulus and Poisson's ratio for similar DLC films as well as tungsten [30–33]. According to Hertzian theory for a spherical tip impacting a flat surface,

$$\frac{1}{E'} = \frac{1-\nu_{DLC}^2}{E_{DLC}} + \frac{1-\nu_W^2}{E_W} \quad (1)$$

$$F_N = \frac{4E' a^3}{3R} \quad (2)$$

$$p_{max} = \frac{1}{\pi} \sqrt{\frac{6F_N E'}{R^2}} \quad (3)$$

Eq. (1) is a determination of the equivalent modulus of the contact, and Eq. (2) is a calculation of the normal load  $F_N$  as a function of contact radius  $a$  and tip radius of curvature  $R$ . We can calculate the maximum contact pressure from Eq. (3). This analysis (which involves measuring  $a$  and  $R$  directly) leads to a contact pressure estimate of 5 GPa for typical tip sizes. However in order to measure the necessary contact areas and tip deformation, much stronger contact than normal had to be made. Therefore we estimate that the actual contact pressures during the experiment are likely less than 1 GPa. For completeness, note that while adhesion will add to the normal load, the effect is small, on the order of tens of nN [34], and for hydrogen-passivated surfaces much less [35]. We can therefore neglect this effect when estimating the forces at the contact.

### 2.3. Electron energy loss spectroscopy

Periodically between sliding passes, the screen was lifted to capture an EELS spectrum. EELS is sensitive to the energy difference between the carbon ionization K-edge  $\sigma^*$  (290 eV, corresponding to  $sp^3$  bonding), and the  $\pi^*$  edge at 286 eV from  $sp^2$  bonded carbon. By measuring the background-subtracted integrated counts from these two edges, the ratio of  $sp^2$  to  $sp^3$  bonds can be determined [36].

In practice, however, the EELS measurement is often dependent on the electron dose [37] and can also depend upon other instrumental parameters such as collection angle, variations in the beam intensity during a long experiment and spectrometer resolution. Therefore some care is needed to be quantitative. We measured the dose rate for each GIF entrance aperture and magnification: the dose rate  $R$  ( $e^-/\text{\AA}^2\text{s}$ ) is given by:

$$R = \frac{B \cdot M^2}{K \cdot A} \quad (4)$$

where  $K$  is the electronic charge,  $B$  the beam current in amperes,  $A$  the collection area on the screen, and  $M$  the magnification. The beam current ( $C/s$ ) itself was measured using the microscope's displayed screen current [38]. The electron counts are then normalized to the lowest dose (i.e. 3 mm GIF entrance aperture) to reflect the fact that high-dose measurements result in  $sp^2/sp^3$  ratios that are higher than they should be.

In addition, we measured a “baseline” of EELS spectra as a function of time on an adjacent region of the sample, without any sliding taking

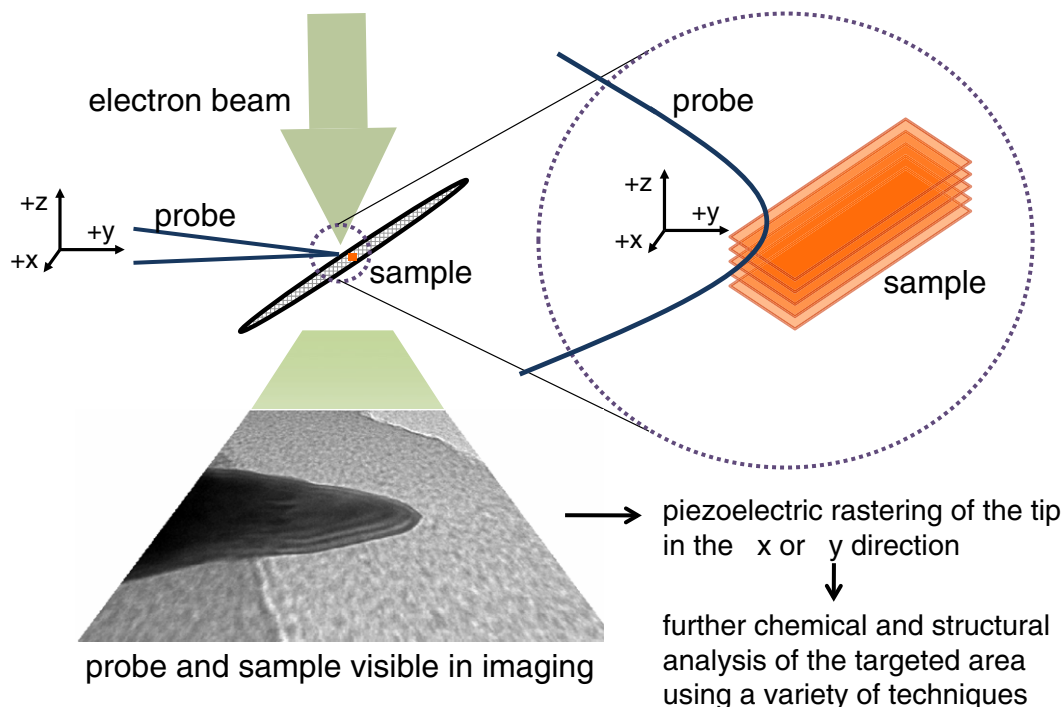


**Fig. 2.** A schematic of the STM-TEM holder inside the microscope column. The TEM micrograph shown represents a typical view of the tip inside the microscope column. X, Y, and Z refer to the motion directions available to the tip, and are not absolute coordinates. The sample itself is mounted in a full-size TEM grid rotated 45° about the x-axis as shown, and the sliding is done in the  $\pm x$  direction.

place. We can subtract this from our sliding results to compensate for the effect of electron irradiation on the sample bonding. In our case we see a decrease in the ratio of  $sp^2$  to  $sp^3$  bonding with increasing exposure time, which could be explained by hydrogen migration (probably caused by broken C–H bonds) or carbon polymerization [39].

The true  $sp^2/sp^3$  bonding ratio can not be directly measured. However, we can safely measure the proportional changes of the  $sp^2$  and  $sp^3$  signal, because of the proportionality of EELS counts to bonding

electrons in the sample [37]. This lets us identify a rate of transformation from  $sp^3$  to  $sp^2$  bonding as a function of the total number of bonds in the film: knowing the sample area dimensions from the corresponding micrographs and the film thickness, we can then calculate the total number of bonding electrons using the density of the film [29]. For our samples, this number is approximately 25,600,000. Then, using the percentage change per minute of  $sp^2$  and  $sp^3$  bonds, and subtracting the baseline rate, we can look at the change in adjusted  $sp^2/sp^3$  counts ratio as a function of time. Finally we can express the results as a number of monolayers representing the total volume transformed should all of the transformation happen at the surface.

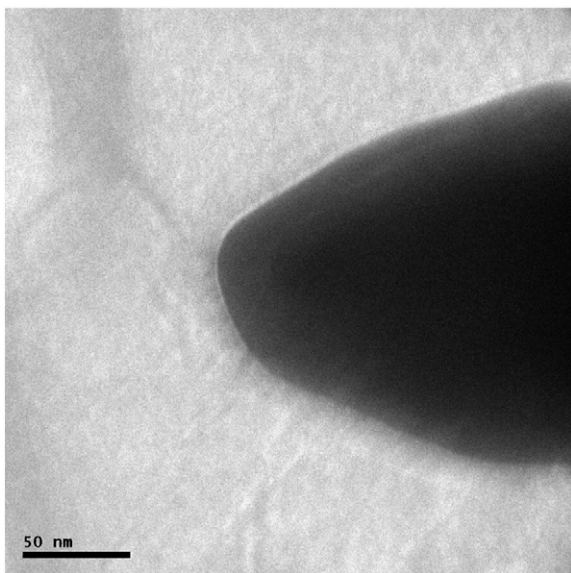


**Fig. 3.** TEM micrograph of a typical tungsten tip before sliding, prepared by electrochemical etching. This is representative of the kind of tips used in the actual sliding experiments.

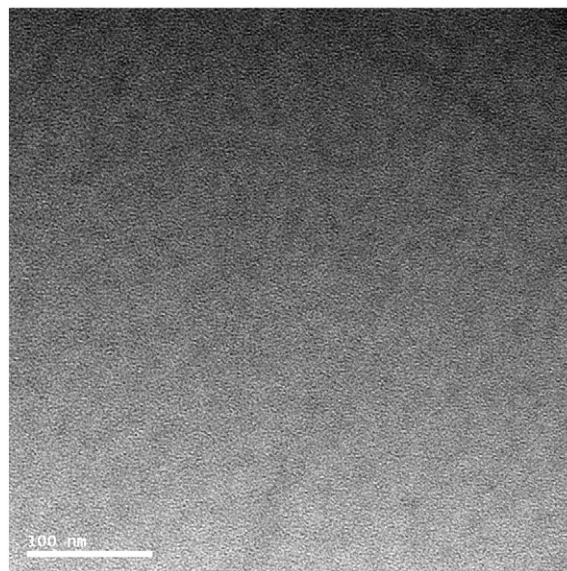


**Fig. 4.** DLC film electron micrograph from a pristine region of the sample.

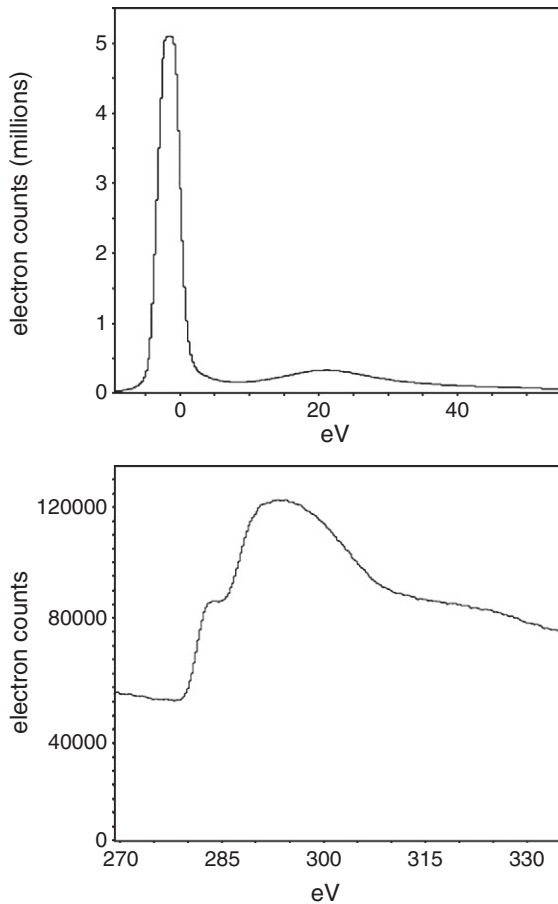


**Fig. 5.** EELS zero-loss and carbon K-edge spectra from the same region of sample shown in Fig. 4. Small amounts of energy shift tend to occur over time, and are taken into account during the analysis of sequential spectra.

By looking at rates of change of the  $1s \rightarrow \pi^*$  edge we avoid issues with dose and aperture effects, as well as those arising from convolution with C–C bonding, C–H bonding, etc. We take the normalized, background-subtracted signal and use a Gaussian fitting method to integrate the counts and quantifiably report the relative differences in these values over the course of an experiment. This also removes the need for us to perform the complex task of calibration and absolute quantification of the EELS data.

EELS spectra, being essentially an electron counting process, should generally exhibit noise following Poisson statistics, although the use of a charge-coupled device camera to record the data slightly complicates this [40]. After calculating the statistical and integration error for the measurements, it was found to be negligible in light of the high numbers of counts collected, and the goodness of fits. However, it is safe to assume larger systematic errors on the order of 5–10%. Significant sources of error include the relatively high background levels which must be subtracted (using a power-law fit), the convolution of the signal with the low-loss spectrum, and the count integration. Each of these three processes must be done by the user and lacking clear standards are subject to human variability.

### 3. Results

Although the variable dose prevented a good absolute measurement of the pi/sigma bonding ratio in the film, the change over time was consistently positive during sliding and consistently negative for the electron beam baseline condition as shown in Fig. 6. The total

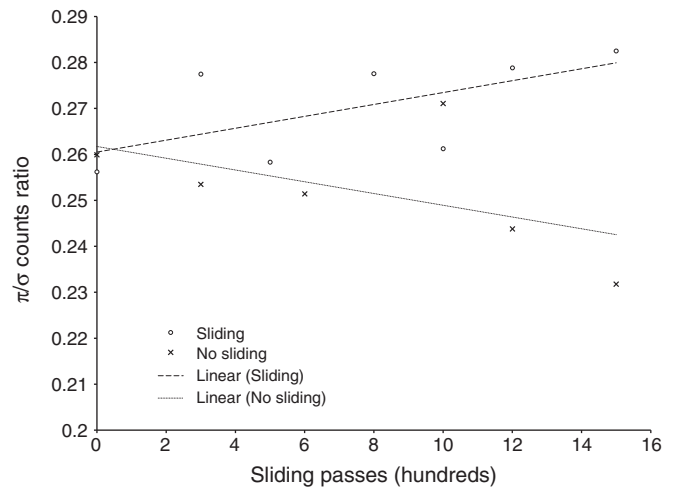


**Fig. 6.** The data points show the ratio of normalized, integrated pi to sigma counts as measured from EELS spectra. Pi counts are representative of  $sp^2$  carbon bonding, and sigma counts are representative of  $sp^3$  bonding. Compared are a typical sliding experiment with a baseline test done without sliding (29.5 nm thickness) under the electron beam.

counts were seen to increase or decrease over the course of the experiment, which we attribute to sample drift, the accumulation of contaminants on the surface, or in general a changing sample volume.

While the exact  $sp^3$  to  $sp^2$  conversion rates varied from sample to sample and even among entrance aperture sizes, our measurements in Fig. 7 show a consistent increasing trend in the  $sp^2$  to  $sp^3$  bonding ratio, with the adjusted pi counts increasing approximately 1% more per minute than the adjusted sigma counts over the course of the experiment. This held for each sample tested, regardless of the increase or decrease in the overall number of counts.

Similar behavior was seen at all the tested areas. Averaging the equivalent monolayers transformed data to a linear trend, we observe a rate of  $sp^3$  to  $sp^2$  transformation between 0.009% and 0.018% of the total sampled volume per pass. Extrapolating these rates under constant

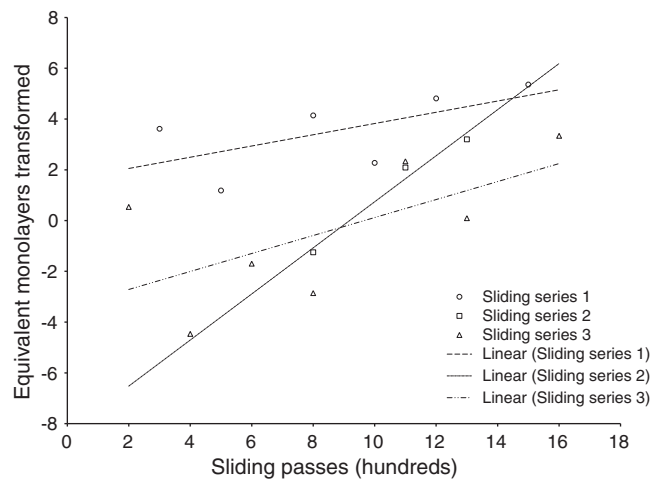


**Fig. 7.** EELS spectra taken during sliding, sample thickness  $\sim 35.2$  nm. The entrance aperture was 3 mm for the first series and 2 mm for the second and third. The data points show the equivalent number of monolayers transformed from  $sp^3$  to  $sp^2$  bonding. Negative values represent a transformation in the opposite direction, something which we attribute to drift and other factors near the beginning of the sliding experiment. A linear regression trendline is shown for the data points measured relative to the initial condition.

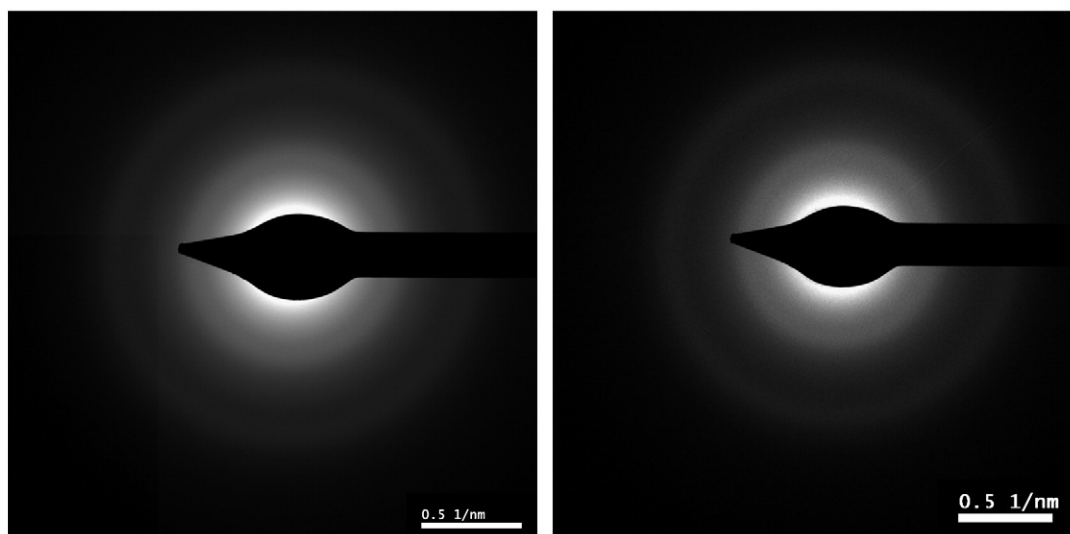


Fig. 8. Nanodiffraction patterns of the same region of film before (left) and after (right) a sliding experiment. The approximate sample area is 800 nm in diameter.

conditions would correspond to transformations of 13.5% to 27% after approximately 30 min of sliding at a given sample volume.

#### 4. Discussion

We can see from the nanodiffraction patterns shown in Fig. 8, as well as the full width at half maximum of the EELS spectra, that from the beginning to the end of the experiment, there was no significant long-range ordering in the sampled volume – which would have been evident in a diffraction spot, sharper rings in the diffraction pattern, and possibly a narrowing of the carbon  $1s \rightarrow \pi^*$  edge. This indicates that localized amorphous regions of  $sp^2$  bonding are forming, as opposed to large regions of crystalline graphite. Since graphite is thermodynamically more stable than amorphous carbon or diamond, any stimulus (mechanical, thermal, etc.) will move the system to the lower free-energy state, hence increased  $sp^2$  content is to be expected. The linear rate of transformation through the end of the experiment suggests that we have not created  $sp^2$  bonds solely on the surface; we can calculate the thickness of a hypothetical  $sp^2$  surface layer, which for the second series was over 12 Å. If the changes in the bonding were limited to the immediate surface, we would expect a decreasing of the transformation rate with sliding which we do not. With more extensive formation of  $sp^2$  bonding due to more deformation, crystalline graphite would be expected to form, consistent with other reports [17–21].

The immediate linear trend of the transformation rate also has implications for the possibility of hydrogen migration contributing to the  $sp^3$ – $sp^2$  transformation. Preliminary results on NFC6 films [21], which contain a much thicker hydrogen-free “dead zone on the top surface” [41], show a nonlinear rate of transformation, initially slow but sharply increasing after a certain time. The N3FC films tested in this study have a much smaller dead zone, perhaps providing a constant migration of hydrogen atoms at the surface from the very beginning of the experiment.

In summary, under the conditions of the experiment herein disordered  $sp^2$  bonding is formed in response to the mechanical stimulus of a sliding tip, the rate being linear with the number of sliding passes.

#### Acknowledgments

The authors acknowledge valuable feedback from Jackie Johnson over the course of this project. The authors would also like to

acknowledge Russell Cook for his technical assistance. The electron microscopy was performed at the Electron Microscopy Center for Materials Research at Argonne National Laboratory, a U.S. Department of Energy Office of Science Laboratory operated under Contract No. DE-AC02-06CH11357 by UChicago Argonne, LLC.

OA and AE acknowledge funding by the U.S. Department of Energy, Office of Energy Efficiency and Renewable Energy, Freedom Car and Vehicle Technologies Program, under Contract no. DE-AC02-06CH11357 and the U.S. Air Force Office of Scientific Research on grant number FA9550-08-1-0010.

AM and LDM acknowledge funding by the National Science Foundation on Grant Number CMMI-1030703.

#### References

- [1] A.C. Ferrari, J. Robertson, *Physical Review B* 61 (2000) 14095.
- [2] A. Erdemir, I.B. Nilufer, O.L. Eryilmaz, M. Beschliesser, G.R. Fenske, *Surface and Coatings Technology* 120–121 (1999) 589.
- [3] A. Erdemir, O.L. Eryilmaz, G. Fenske, *Journal of Vacuum Science & Technology A* 18 (2000) 1987.
- [4] C. Donnet, A. Erdemir, *Surface & Coatings Technology* 180–81 (2004) 76.
- [5] A. Erdemir, *Tribology International* 38 (2005) 249.
- [6] A. Erdemir, *Tribology International* 37 (2004) 1005.
- [7] J. Andersson, R.A. Erck, A. Erdemir, *Wear* 254 (2003) 1070.
- [8] J.A. Heimberg, K.J. Wahl, I.L. Singer, A. Erdemir, *Applied Physics Letters* 78 (2001) 2449.
- [9] C. Donnet, T.L. Mogne, L. Ponsonnet, M. Belin, A. Grill, V. Patel, C. Jahnnes, *Tribology Letters* 4 (1998) 259.
- [10] J.C. Sánchez-López, M. Belin, C. Donnet, C. Quirós, E. Elizalde, *Surface and Coatings Technology* 160 (2002) 138.
- [11] J.C. Sánchez-López, A. Erdemir, C. Donnet, T.C. Rojas, *Surface and Coatings Technology* 163–164 (2003) 444.
- [12] A. Erdemir, *Surface and Coatings Technology* 146–147 (2001) 292.
- [13] A. Erdemir, O.L. Eryilmaz, I.B. Nilufer, G.R. Fenske, *Diamond and Related Materials* 9 (2000) 632.
- [14] A.A. Voevodin, A.W. Phelps, J.S. Zabinski, M.S. Donley, *Diamond and Related Materials* 5 (1996) 1264.
- [15] J.A. Harrison, C.T. White, R.J. Colton, D.W. Brenner, *Physical Review B* 46 (1992) 9700.
- [16] J.A. Harrison, C.T. White, R.J. Colton, D.W. Brenner, *Thin Solid Films* 260 (1995) 205.
- [17] Y. Liu, A. Erdemir, E.I. Meletis, *Surface & Coatings Technology* 86–7 (1996) 564.
- [18] Y. Liu, A. Erdemir, E.I. Meletis, *Surface and Coatings Technology* 82 (1996) 48.
- [19] K. Kanda, N. Yamada, M. Okada, J.-y. Igaki, R. Kometani, S. Matsui, *Diamond and Related Materials* 18 (2009) 490.
- [20] A.V. Sumant, D.S. Grierson, J.E. Gerbi, J.A. Carlisle, O. Auciello, R.W. Carpick, *Physical Review B (Condensed Matter and Materials Physics)* 76 (2007) 235429–235411.
- [21] A.P. Merkle, A. Erdemir, O.L. Eryilmaz, J.A. Johnson, L.D. Marks, *Carbon* 48 (2010) 587.
- [22] A.P. Merkle, L.D. Marks, *Wear* 265 (2008) 1864.
- [23] L.D. Marks, O.L. Warren, A.M. Minor, A.P. Merkle, *MRS Bulletin* 33 (2008) 1168.

- [24] A.P. Merkle, L.D. Marks, *Applied Physics Letters* 90 (2007) 064101.
- [25] Y. Liao, S.K. EswaraMoorthy, L.D. Marks, *Philosophical Magazine Letters* 90 (2010) 219.
- [26] A. Merkle, L. Marks, *Microscopy and Microanalysis* 12 (2006) 950.
- [27] A. Merkle, L.D. Marks, *Applied Physics Letters* 90 (2007) 64101.
- [28] O.L. Eryilmaz, A. Erdemir, *Wear* 265 (2008) 244.
- [29] D. Shindo, T. Musashi, Y. Ikematsu, Y. Murakami, N. Nakamura, H. Chiba, *J Electron Microsc (Tokyo)* 54 (2005) 11.
- [30] E. Martínez, J.L. Andújar, M.C. Polo, J. Esteve, J. Robertson, W.I. Milne, *Diamond and Related Materials* 10 (2001) 145.
- [31] S.-J. Cho, K.-R. Lee, K. Yong Eun, J. Hee Hahn, D.-H. Ko, *Thin Solid Films* 341 (1999) 207.
- [32] J.A. Johnson, *Journal of Applied Physics* 95 (2004) 7765.
- [33] B.C. Yeldose, B. Ramamoorthy, *The International Journal of Advanced Manufacturing Technology* 38 (2007) 705.
- [34] B. Bhushan, C. Dandavate, *Journal of Applied Physics* 87 (2000) 1201.
- [35] R.W. Carpick, E.E. Flater, K. Sridharan, *Polymeric Materials Science and Engineering* (2004) 198.
- [36] S.D. Berger, D.R. McKenzie, P.J. Martin, *Philosophical Magazine Letters* 57 (1988) 285.
- [37] L. Ponsonnet, C. Donnet, K. Varlot, J.M. Martin, A. Grill, V. Patel, *Thin Solid Films* 319 (1998) 97.
- [38] F.E.I. Company, *Tecnai F20/F30 Operating Manual*, FEI Company, The Netherlands, 1999.
- [39] D. Adliene, J. Laurikaitiene, V. Kopustinskas, S. Meskinis, V. Sablinskas, *Materials Science and Engineering: B* 152 (2008) 91.
- [40] J. Verbeeck, S. Van Aert, *Ultramicroscopy* 101 (2004) 207.
- [41] J.A. Johnson, D. Holland, J.B. Woodford, A. Zinovev, I.A. Gee, O.L. Eryilmaz, A. Erdemir, *Diamond and Related Materials* 16 (2007) 209.